

On the synthesis of vanadium containing molecular sieves by experimental design from a $\text{VOSO}_4 \cdot 5\text{H}_2\text{O} \cdot \text{Al}(\text{iPrO})_3 \cdot \text{Pr}_2\text{NH} \cdot \text{H}_2\text{O}$ gel: occurrence of VAPO-41 as a secondary structure in the synthesis of VAPO-11

Ligia Frunza^{a,1}, Pascal Van Der Voort^b, Etienne F. Vansant^b, Robert A. Schoonheydt^a, Bert M. Weckhuysen^{a,*}

^a *Departement Interfasechemie, Centrum voor Oppervlaktechemie en Katalyse, K.U. Leuven, Kardinaal Mercierlaan 92, 3001 Heverlee, Belgium*

^b *Laboratorium voor Anorganische Scheikunde, Department Scheikunde, U.I. Antwerpen, Universiteitsplein 1, 2610 Wilrijk, Belgium*

Received 14 December 1999; received in revised form 25 April 2000; accepted 26 April 2000

Abstract

An experimental design was applied to the hydrothermal synthesis of VAPO-11 molecular sieve (AEL structure) from a $\text{VOSO}_4 \cdot 5\text{H}_2\text{O} \cdot \text{Al}(\text{iPrO})_3 \cdot \text{Pr}_2\text{NH} \cdot \text{H}_2\text{O}$ gel. The influence of five synthesis parameters (synthesis temperature, synthesis time, vanadium content, water content and template content) on the crystallinity and physicochemical properties of the as-synthesized materials was studied. The obtained materials were characterized by electron spin resonance (ESR), diffuse reflectance spectroscopy (DRS), X-ray diffraction, thermal analysis measurements, scanning electron microscopy and in situ Fourier transform infrared (FTIR) spectroscopy. The AEL structure appears either as a single phase or as a physical mixture together with the AFO structure (VAPO-41). A statistical model is proposed, which relates the synthesis variables with the crystallinity allowing to indicate the optimal synthesis conditions for VAPO-11. Highly crystalline single-phase VAPO-11 can be best prepared at 170°C from a synthesis gel with a low vanadium content (0.02 mol) and a high water content (25 mol). The co-ordination of vanadium in these materials is discussed on the basis of the ESR and DRS spectra. The spectroscopic data are explained by the presence of a vanadium species in distorted octahedral co-ordination, composed of two V–O–T bonds with the framework, one bond with the vanadyl oxygen and three water molecules as ligands. © 2000 Elsevier Science B.V. All rights reserved.

Keywords: Experimental design; VAPO-11; VAPO-41; Synthesis and characterization

1. Introduction

Since the discovery of aluminophosphate molecular sieves (AlPO-*n*) in 1982 [1], a large number of framework structure types have been described in the literature [2]. Framework Al and/or P can be replaced by Si [3] or by transition metal ions [4],

* Corresponding author.

E-mail address: bert.weckhuysen@agr.kuleuven.ac.be (B.M. Weckhuysen).

¹ On leave from the National Institute of Materials Physics, P.O. Box Mg 07, R-76900 Bucharest-Magurele, Romania.

leading to materials with interesting catalytic and/or adsorptive properties. In the previous studies the incorporation of vanadium is reported in several aluminophosphate structures such as AFI, ATO, AFO, AEL, VFI, AFS, FAU, AFR [5,6], some of them being active in the oxidation reactions of organic compounds [7–10].

Nowadays, there is a growing interest in finding a more rational approach towards the synthesis of molecular sieves. An attractive example for such approaches is the use of combinatorial methods for fast screening of a large number of synthesis mixtures [11–14]. Another approach is based on the concepts of experimental design. It has been used in our laboratory [15] and by other groups [16–19] and a many-variable-at-a-time approach is followed, in which several synthesis variables are changed at the same time, leading to a significant reduction in the number of synthesis trials. Thus, the method has been explored for the synthesis of CoAPO-11, -44 and -46 from a $\text{Co}(\text{Ac})_2 \cdot 4\text{H}_2\text{O} \cdot \text{Al}(\text{iPrO})_3 \cdot \text{Pr}_2\text{NH} \cdot \text{H}_2\text{O}$ gel [15]. The influence of the synthesis time, synthesis temperature, the amount of cobalt, the amount of template and the amount of water, on the hydrothermal synthesis was studied, and a model relating the overall crystallinity with the experimental parameters and with the degree of the isomorphous substitution of Co^{2+} was developed.

In this work, we have extended our experimental design approach to the hydrothermal synthesis of VAPO-11 and VAPO-41 from a $\text{VOSO}_4 \cdot 5\text{H}_2\text{O} \cdot \text{Al}(\text{iPrO})_3 \cdot \text{Pr}_2\text{NH} \cdot \text{H}_2\text{O}$ gel. The selection of these systems was based on the similarity in structure and synthesis conditions. Indeed, both structures can be obtained hydrothermally using di-*n*-propylamine (Pr_2NH) as template [3]. In addition, AEL and AFO are both medium pore molecular sieves having elliptical 10-ring channels, and their structures are built from 4- and 6-rings as secondary building units [20,21]. They have the same theoretically calculated framework energy of 4.1 kJ/mol of framework tetrahedra TO_2 [22], which is in good agreement with the experimental thermochemical data of Navrotsky [23], and a very similar framework density (19.1 and 19.0 T atoms per 1000 Å³). Obtaining vanadium containing AEL and AFO materials as single crystalline

phases is a scientific challenge, which requires the proper choice and control of the synthesis parameters.

Five synthesis parameters have been studied in this work: synthesis temperature, synthesis time, vanadium content, water content and template content. Since ESR and DRS have been shown to be useful techniques for characterizing vanadium in molecular sieves [24,25], we have used these techniques alongwith others, such as X-ray diffraction (XRD), thermal analysis measurements (TGA-DTA), scanning electron microscopy (SEM), in situ Fourier transform infrared (FTIR) spectroscopy, in order to characterize the as-synthesized materials. It will be shown that the AEL structure can be obtained, either as single phase or as physical mixtures with different relative proportions of AEL and AFO. A statistical model is proposed which relates the variables with the crystallinity allowing to indicate the optimal synthesis conditions for VAPO-11 materials. In addition, we observed that, independent of the structure type, vanadium ions are present in the framework in distorted octahedral coordination, most probably with three water molecules as ligands.

2. Experimental

2.1. Experimental design

In the first step of the experimental design, we selected five factors that influence the synthesis of vanadium containing aluminophosphate molecular sieves, based on the literature results concerning the formation of the AFO and AEL structures [26–28]. In order to find a correlation among these factors and the overall crystallinity of vanadium containing aluminophosphates, we used the software MODDE for WINDOWS 3.0 (Umetri AB). The five factors or design variables are as follows: X_1 , the synthesis time (h); X_2 , the synthesis temperature (K); X_3 or y , the water content (mol); X_4 or x , the vanadium content (mol) and X_5 or r , the template content (mol). The gel composition was $\text{V}_x\text{Al}_{1-x}\text{PO}_4 \cdot y\text{H}_2\text{O} \cdot r\text{Pr}_2\text{NH}$. The limits of variation for each factor were as follows: X_1 , 16.8–67.2 h;

X_2 , 437–479 K; X_3 , 10–28 mol H_2O ; X_4 , 0.008–0.092 mol of vanadium; X_5 , 0.4–1.1 mol of template. Consequently, a set of 29 experiments resulted, in which each factor can take three distinct values, a central one and two limits. The spreadsheet generated by MODDE is presented in Table 1 along with the crystallinity degree of the samples and the phase identification in the as-synthesized materials. The reproducibility of the synthesis process is given by the two replicate points N28 and N29 of the central point N27 in the experimental design.

2.2. Sample preparation

29 Synthesis gels for vanadium containing aluminophosphate molecular sieves were prepared according to the parameters of the experimental design given in Table 1. The general procedure is as follows: the vanadium salt was added to a solution of H_3PO_4 in water, followed by adding the aluminum source under continuous stirring. After obtaining a homogeneous mixture, the template was added dropwise under continuous stirring. The homogeneous synthesis gel was then transferred into a Teflon-lined autoclave. The synthesis was performed as given by the experimental design procedure of Table 1. After synthesis, the solid material was recovered from the synthesis mixture by centrifugation, washed three times with bidistilled water, dried at 333 K overnight in an oven and stored under ambient conditions. To remove the organic template, the as-synthesized samples were calcined overnight at 773 K in air.

In order to obtain a pure VAPO-41 phase, a separate synthesis had to be performed, according to the procedure reported by Kevan et al. [27]. For comparison purposes, a VAPO-5 material was synthesized following an earlier reported recipe [24]. Additionally, a high crystalline VAPO-11 sample was obtained using known procedures [28], which is considered as standard for evaluating the XRD crystallinity degree.

The following chemicals were used as received for the molecular sieve syntheses: aluminum triisopropoxide (Acros Organics, 98+%), H_3PO_4 85 wt.% (Janssen, p.a.), di-*n*-propylamine (Janssen,

p.a.) and vanadyl sulfate $VOSO_4 \cdot 5H_2O$ (Merck, p.a.).

Vanadyl containing silica gel samples were prepared for developing a V^{4+} ESR calibration line. These samples were obtained by impregnating silica gel 60 (Fluka) with aqueous solutions of vanadyl sulfate [29]. The samples were dried at 333 K in air and stored under ambient conditions.

2.3. Sample characterization

X-ray powder diffractograms were obtained using a Siemens D5000 diffractometer with CuK_α radiation. The XRD overall crystallinity was estimated from the highest diffraction peak or as the sum of the intensities of some of the most characteristic peaks of each individual crystalline phase as follows: peaks at $2\theta = 8.10, 13.08$ and 15.80° for the AEL structure and peaks at $2\theta = 6.85, 13.72$ and 18.26° for the AFO structure.

ESR spectra were recorded at 120 and/or 300 K with a Bruker ESP300E spectrometer in the X-band (9.5 GHz). The modulation frequency and the modulation amplitude were, respectively, 100 kHz and 5 G. The same volume (“standard”) of sample, accurately weighed, was used for each spectral measurement to minimize inaccuracies due to the variation of sensitivity with position in the ESR cavity. Moreover, this known volume was used also for the series of ESR calibrating V^{4+}/SiO_2 samples. Double integration was performed in order to quantify the ESR signals. The ESR spectra were simulated with the program SIMPOW of Mark Nilges; it generates a powder spectrum calculated to second order, for one metal nucleus with a spin 1/2 or greater and three superhyperfine spins for which there can be more than one equivalent nucleus.²

Scanning electron microscopy was performed with a Phillips 515 microscope on samples deposited onto an alumina support and coated with a gold film.

² Spectral optimization software was provided by the Illinois ESR Research Center, NIH Division of research, grant RR01811, that includes the algorithm developed by Mattson et al. [30].

Table 1
Five-level circumscribed central composite experimental design for the hydrothermal synthesis of VAPO materials

Experiment no.	Experiment name	Run order	Time (h)	Temperature (K)	H ₂ O (mol)	Vanadium (mol)	Template (mol)	Crystallinity degree of AEL phase ^a	Other XRD phases	Phase purity <i>R</i> of AEL ^b
1	N1	16	24	443	10	0.02	1	0	–	0
2	N2	6	60	443	10	0.02	0.5	0	–	0
3	N3	4	24	473	10	0.02	0.5	0.63	AFO	6.5
4	N4	3	60	473	10	0.02	1	0.29	AFO	0.8
5	N5	1	24	443	25	0.02	0.5	0.57	–	∞
6	N6	15	60	443	25	0.02	1	0.73	–	∞
7	N7	22	24	473	25	0.02	1	0	–	0
8	N8	18	60	473	25	0.02	0.5	0.79	AFO	9.8
9	N9	2	24	443	10	0.08	0.5	0.41	AFO	1.38
10	N10	14	60	443	10	0.08	1	0	–	0
11	N11	29	24	473	10	0.08	1	0	–	0
12	N12	12	60	473	10	0.08	0.5	0.56	AFO	7.66
13	N13	5	24	443	25	0.08	1	0.27	AFO	0.05
14	N14	19	60	443	25	0.08	0.5	0.51	AFO	3.96
15	N15	23	24	473	25	0.08	0.5	0.46	AFO	6.5
16	N16	28	60	473	25	0.08	1	0	–	0
17	N17	25	16.8	458	17.5	0.05	0.75	0.23	–	∞
18	N18	20	67.2	458	17.5	0.05	0.75	0.41	AFO	0.56
19	N19	9	42	437	17.5	0.05	0.75	0.39	AFO	0.5
20	N20	26	42	479	17.5	0.05	0.75	0.56	AFO	2.99
21	N21	7	42	458	7	0.05	0.75	0	T,C ^c	0
22	N22	21	42	458	28	0.05	0.75	0.47	AFO	2.5
23	N23	8	42	458	17.5	0.008	0.75	0.30	AFO	1
24	N24	13	42	458	17.5	0.092	0.75	0.32	AFO	2
25	N25	11	42	458	17.5	0.05	0.4	0.17	–	∞
26	N26	17	42	458	17.5	0.05	1.1	0.34	AFO	0.66
27	N27	10	42	458	17.5	0.05	0.75	0.67	AFO	1.67
28	N28	24	42	458	17.5	0.05	0.75	0.56	AFO	1.65
29	N29	27	42	458	17.5	0.05	0.75	0.64	AFO	1.74

^a This value was calculated as the ratio of the sum of the intensities of three main peaks ($2\theta = 8.10, 13.08, 15.80^\circ$) in the pattern of the given sample and of the standard sample.

^b *R* is the ratio of the intensities of the peaks at $2\theta = 8.10$ and 6.85° of AEL and AFO, respectively.

^c Tridymite/cristobalite structure.

Thermal analysis measurements were carried out using a Setaram TG-DTA92 apparatus in helium/oxygen flow at a heating rate of 5 K/min.

In situ FTIR spectroscopy was used to observe the water and template removal from the as-synthesized materials, evacuated under vacuum upon increasing the temperature. For this purpose, self-supporting wafers of the material under study were introduced in a quartz cell and evacuated under vacuum (1 Pa). The spectra were recorded with a Nicolet 750 FTIR apparatus in the range 400–4000 cm^{-1} for different desorption temperatures.

Diffuse reflectance spectra in the UV–VIS–NIR region were recorded on a Varian Cary 5 spectrometer against a Halon white standard. The spectra were recorded in air at room temperature. When necessary, the samples were diluted in order to normalize the spectra to the same amount of vanadium. Reflectance data were converted to absorption spectra using the Kubelka–Munk function $F(R_\infty)$. The absorption edge in the UV–visible spectra was determined for calcined samples, using the Tauc law, from the intercept of the function $[F(R_\infty)h\nu]^2$ plotted versus $h\nu$, the energy of incident photon.

Elemental analysis was performed with a Perkin–Elmer 3000 ICP instrument. A weighed amount of the sample was dissolved in hot nitric acid until the dissolution was complete and the clear solution was diluted to ~3% (v/v nitric acid) prior to ICP analysis.

3. Results and discussion

3.1. Synthesis of VAPO-11 materials

The initial synthesis gels were blue or light blue depending on the vanadium content, while the as-synthesized samples were mostly light-green and grey, and also yellowish when the vanadium content was higher. All the calcined samples were light-yellow to yellow, due to oxidation of V^{4+} to V^{5+} .

The crystallinity of the samples and the phase identification were evaluated from XRD patterns, and the results are presented in Table 1. A single

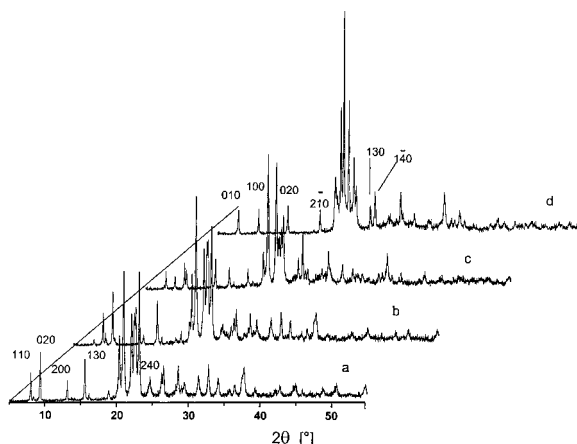


Fig. 1. XRD patterns of as-synthesized VAPO molecular sieves: (a) sample N6, (b) sample N8, (c) sample N9, and (d) sample VAPO-41.

phase of the AEL type was obtained only in the case of the samples N5, N6, N17 and N25 (in the latter two cases even with low crystallinity), and the corresponding XRD diffractograms are typical for the AEL structure [21] both with respect to the peak positions and intensities (Fig. 1, curve a). The majority of the samples consist of a mixture of the phases AFO and AEL. Examples are given in Fig. 1 (curves b and c). The (hkl) peaks characteristic of the AEL topology at $2\theta = 8.09$ (1 1 0), 13.14 (2 0 0) and 15.66° (1 3 0) decrease in intensity when passing from sample N6 to samples N8 and N9. At the same time, the reflections characteristic for the AFO structures are clearly developed at 6.85 (0 1 0), 13.72 (0 2 0), 18.26 (2 -1 0) and $\sim 25^\circ$ (1 3 0) and (1 -4 0). The XRD pattern of the VAPO-41 sample is also characteristic for AFO materials [15]. Dense phases with tridymite and cristobalite structures were also obtained (sample N21 in Table 1). Six samples were amorphous.

SEM analysis confirmed the crystallinity of the samples. Different morphologies, characteristic for each structure were obtained, in agreement with the literature [27,32]. The pictures of representative polycrystalline aggregates obtained in our study are given in Fig. 2. Rather big spherical aggregates of plates arranged about a central point can be observed for AEL (sample N6), but in the mixture of phases as in sample N26 (Fig. 2b), the

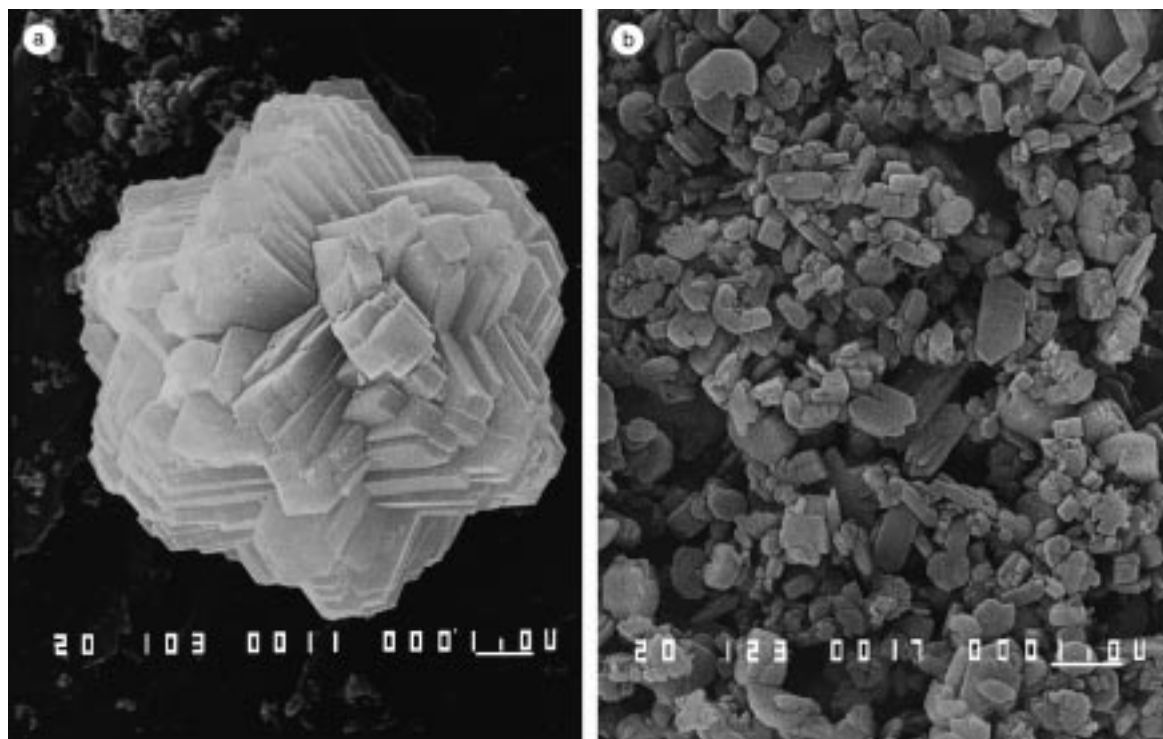


Fig. 2. SEM pictures of (a) sample N6 and (b) sample N26.

rectangular morphology of AFO crystallites also appears.

Elemental analysis of the obtained solids indicates that vanadium is indeed incorporated into the aluminophosphate molecular sieves in about 40–80% from the total amount of V offered. The lower this amount, the higher the percentage of vanadium incorporated in the final solid. A percentage of 40–50% of vanadium incorporated from the total amount offered has been previously observed for VAPO-11 [33]. However, one could not obtain unambiguous evidence for the isomorphous substitution of vanadium into the framework of VAPO materials only by elemental analysis: Thus, a molar ratio $([V] + [Al])/[P] = 1$ is expected in the case that vanadium substitutes for aluminum, while $([V] + [P])/[Al] = 1$ would be typical for substitution for phosphorus. We found that $([V] + [Al])/[P]$ varies between 0.858 and 0.965, so that the molar relationship was not fulfilled in most cases. The values obtained (smaller than 1)

show that most probably extra-framework species are present.

The ESR technique was used to quantify the vanadium concentration in the VAPO materials by double integration of the corresponding ESR spectrum. A calibration curve has been obtained and is presented in Fig. 3a. The ESR intensity of the calibration curve covers the intensity domain of our VAPO samples; it increases linearly with the V loading up to ~ 0.9 mg. At higher V loading, the ESR spectra show an additional broad signal, due to magnetically interacting vanadium species, as vicinal positions in surface polymeric species [34].

The amount of vanadium resulting from the ESR spectra is close to the value found by elemental analysis at low V loading (Fig. 3b), but a comparison of the vanadium amount offered at the synthesis stage and the amount of ESR visible V^{4+} clearly shows that the amount of ESR visible V^{4+} is always much lower than the amount of V^{4+} offered to the synthesis gel.

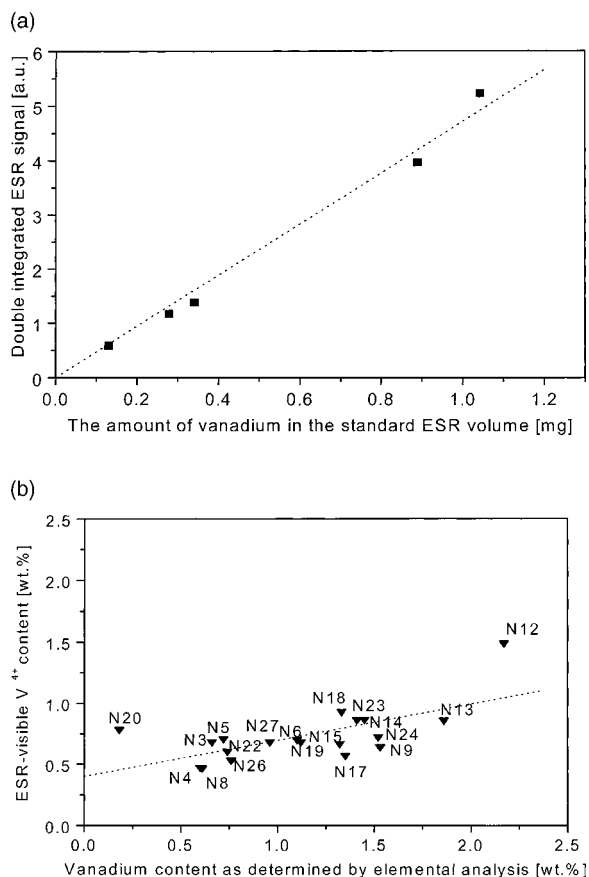


Fig. 3. Vanadium incorporation in the VAPO materials: (a) ESR calibration curve – ESR intensity as a function of the vanadium amount, (b) comparison of the vanadium amount determined by ESR and elemental analysis. The dotted lines represent the least-squares fit at the corresponding data: (a) $y = 4.712x$ ($R = 0.99504$, $SD = 0.23745$, $p < 0.0001$); (b) $y = 0.39967 + 0.29709x$ ($R = 0.65273$, $SD = 0.17529$, $p = 0.00245$).

The water and template content of the as-synthesized samples was determined by thermal analysis. Typical patterns of weight loss and heat flow are presented in Fig. 4A and B, respectively. For the AlPO materials, the oxidative decomposition of the template molecules generally takes place in several stages [33], and exothermal peaks are observed. The elimination of the neutral amine starts at around 573 K, whereas another fraction of the template molecules is burned-off at temperatures higher than 773 K. The latter originates

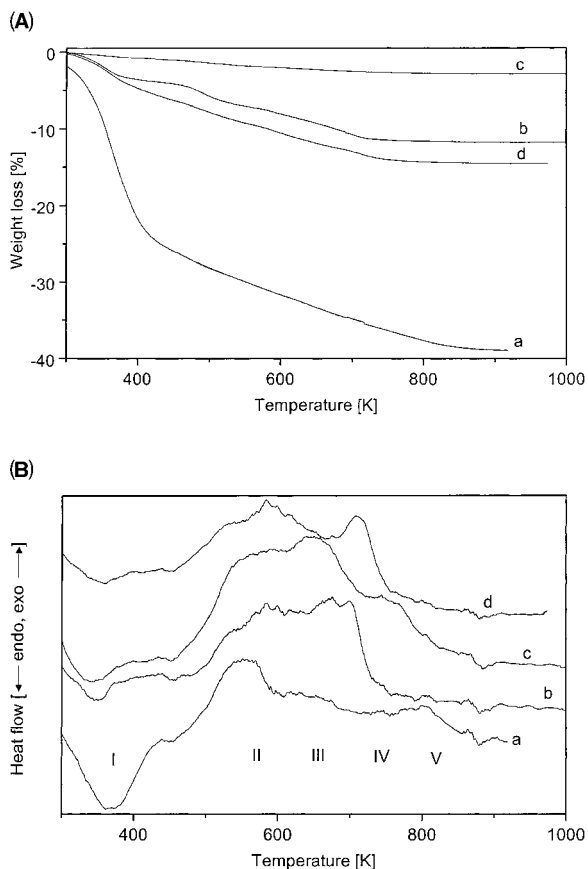


Fig. 4. (A) TGA and (B) DTA curves of as-synthesized VAPO materials: (a) sample N1, (b) sample N6, (c) sample N8 and (d) sample N9.

from the protonated forms strongly interacting with the framework. Since our vanadium containing aluminophosphate samples do not show DTA peaks corresponding to this last stage of template removal, we assume that they do not possess a significant amount of protonated template.

The weight loss corresponding to the endotherm at temperatures between 293 and 473 K is very high in the case of amorphous samples and less important for the well-crystallized samples. However, a careful examination of the TGA curves in correlation with the DTA patterns reveals that for the AEL and/or mixed AEL–AFO samples, this weight loss due to water desorption actually occurs in two steps, which might be consistent with

the fact that the AEL structure contains both water molecules co-ordinated to the framework Al [35] and physisorbed water. It is generally accepted that physisorbed water is removed at ~ 353 K, but the endothermal peak situated among 353 and 473 K has been assigned to the template desorption [7], template decomposition [15] and water desorption [32–37]. The specific assignments are dependent on the template molecule [38] as well as on the framework topology of the molecular sieve.

To make a correct assignment of the endothermal peak at 353–473 K, we performed an in situ infrared study of the calcination process of the as-synthesized material N6. The most relevant IR spectra obtained for increasing calcination temperature are presented in Fig. 5 together with the most important assignments. When the desorption temperature increases from room temperature to 523 K, the spectra change dramatically, especially in the region of the OH stretching vibrations [39], as expected if water is supposed to be desorbed. Even though the exact changes in the intensity of the template peaks appearing in the domains of symmetrical and asymmetrical stretching of C–H and N–H bonds, respectively, as well as in the

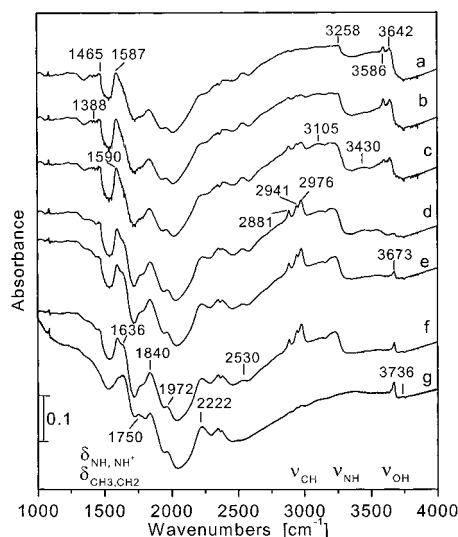


Fig. 5. FTIR spectra of as-synthesized sample N6 for different desorption temperatures: (a) 298 K, (b) 333 K, (c) 433 K, (d) 473 K, (e) 523 K, (f) 548 K and (g) 573 K.

Table 2

Water and template molecules for a unit cell in as-synthesized VAPO samples

Sample	Water/uc ^a	Template/uc ^a
N1	12.9	2.6
N3	5.6	1.4
N6	3.6	1.5
N8	7.3	1.3
N9	4.3	1.8
N12	3.2	1.7
N16	13.5	3.8
N18	7.9	2.2
N19	4.4	2.1
N20	4.2	1.2
N23	5.2	1.6
N24	3.2	1.3
N26	4.6	1.7

^a In the case of amorphous samples, the uc represents an amount of dry sample equivalent to the molecular weight of AEL.

domain of the deformation vibrations of the CH₃, CH₂ and NH groups can be hardly appreciated due to changes in the overall baseline of the spectra, it is however obvious that the template is not desorbed till 473 K, but disappears almost totally at 573 K.

Therefore, we assume that the water is desorbed in the range 298–493 K, while the template is desorbed at higher temperatures. The corresponding amount of water was considered when calculating the number of water molecules per unit cell, as given in Table 2, together with the number of template molecules. The number of template molecules is 5–10 times lower than the amount offered at synthesis stage. The values of Table 2 are in good agreement with those reported in the literature: indeed, a weight loss of about 4% water and 8% template was observed for AlPO-41 [40] (which corresponds, respectively, to ~ 6 and ~ 2 molecules per unit cell); about two template molecules were found in the SAPO-11 unit cell but only 1.3 in SAPO-41 materials [41].

3.2. Optimal conditions for VAPO-11 synthesis

After the completion of the 29 synthesis recipes of Table 1, one can try to relate the crystallinity of the obtained materials with the different synthesis

variables. The necessary methodology has been described in detail in a previous paper [15]. The applied approach is known as the response surface modelling (RSM) method in which a non-linear relation between the characteristic under study (response y) and the factors X_i is modeled by means of a polynomial of the form:

$$y = \beta_0 + \sum_{i=1}^5 \beta_i X_i + \sum_{i \neq j} \beta_{ij} X_i X_j + \sum_{i=1}^5 \beta_{ii} X_i^2,$$

where β_0 is a constant; β_i , the model coefficients for each factor and β_{ii} , the model coefficients of the quadratic terms. In the present investigation, the variable R , which is equal to the ratio of the crystallinity of VAPO-11 over the crystallinity of VAPO-41, is the response y , while the factors X_i are the synthesis variables. Thus, R is a measure of the phase purity of the VAPO-11 sample and the values are included in Table 1. The higher R , the less VAPO-41 is present in the VAPO-11 sample. Values of the different model parameters can then be obtained by using the least-squares method. The significance of the model parameters can be validated by calculating the p value for each model parameter. The p value is defined as the probability to obtain the value of the model coefficient if its own value is zero. Only values with a p value of 0.05 or smaller are considered as statistically significant within a 95% confidence interval. The goodness of fit between model and experiment can be estimated with the R^2 and Q^2 values. R^2 is defined as the percentage of the variation of the response explained by the model, while Q^2 is the predictive power of the model. R^2 and Q^2 are preferentially close to 1.

We obtained a statistically meaningful model with an R^2 value of 0.83 and a Q^2 value of 0.53. The model parameters are summarized in Table 3. Most parameters have excellent p values, which reconfirms the meaningfulness of the model. It is also clear that the model obtained will be less predictive when dealing with the synthesis time and temperature (due to the high p values for β_1 and β_2). The relation between the phase purity R of the series of materials prepared and the synthesis parameters is given by the following equation:

Table 3

Optimized model coefficients β and the p values for the phase purity of the VAPO-11 material

Model coefficient	Scaled and centered value	p value
β_0	0.958	0.395
β_1	0.433	0.622
β_2	-1.034	0.246
β_3	2.883	3.632×10^{-3}
β_4	-2.319	0.015
β_5	-3.468	8.033×10^{-4}
β_{55}	4.975	6.934×10^{-4}
β_{15}	2.735	0.011
β_{23}	-3.202	3.749×10^{-3}
β_{24}	2.607	0.014
β_{34}	-3.193	3.836×10^{-3}

$$R = 0.958 + 0.433X_1 - 1.034X_2 + 2.883X_3 - 2.319X_4 - 3.468X_5 + 4.975X_5^2 + 2.735X_1X_5 - 3.202X_2X_3 + 2.607X_2X_4 - 3.193X_3X_4.$$

In order to visualize this equation, surface plots can be made. Three examples of such surface plots are given in Fig. 6. Fig. 6a shows that phase purity of the VAPO-11 sample increases with increasing synthesis time and decreasing synthesis temperature for a fixed gel composition. As was already pointed out, there is an uncertainty on the curvature of this surface plot, but the trend is statistically correct; i.e., β_1 is positive, whereas β_2 is negative. Thus, VAPO-11 materials are best made from a synthesis gel autoclaved at relatively low temperature (e.g. 170°C) and for long synthesis times (e.g. 60 h). One can conclude from Fig. 6b and c that the most crystalline and phase-pure VAPO-11 materials can be made with a synthesis gel containing a low vanadium content (i.e. 0.02 mol), a high water content (i.e. 25 mol) and a high or low template content (i.e. 0.5 or 1.0 mol). These conclusions are in line with the results obtained from Table 1. Indeed, the sample N6 is the most crystalline among the four synthesized single-phase VAPO-11 samples (N5, N6, N17 and N25). This VAPO-11 material is made from a synthesis gel with 0.02 mol vanadium, 25 mol water and 1 mol template autoclaved at 170°C for 60 h.

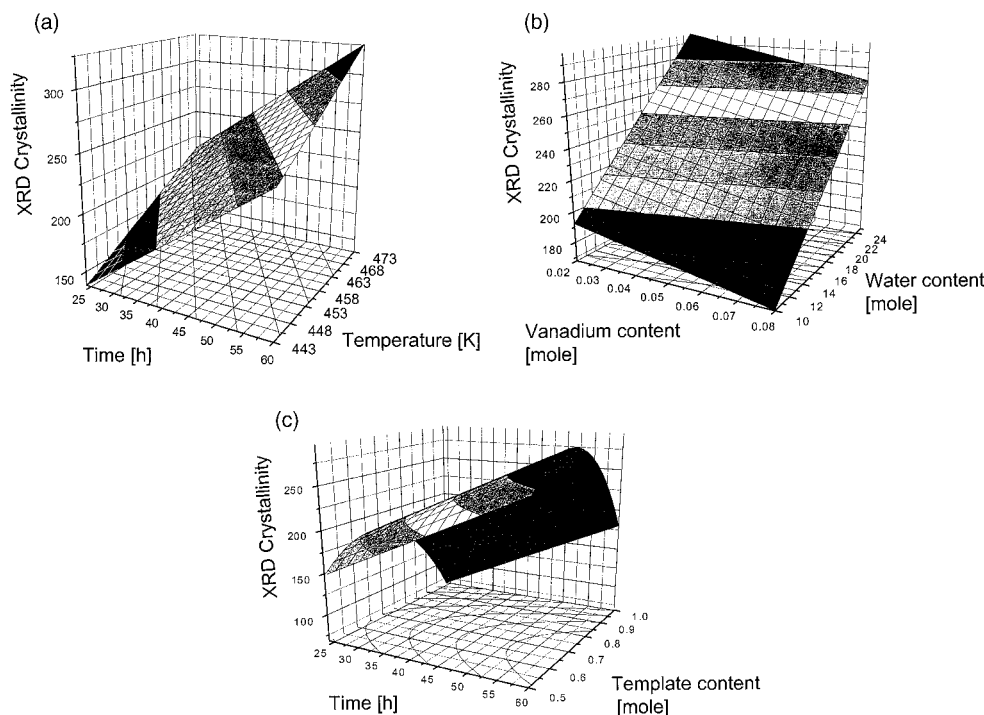


Fig. 6. Phase purity R of the VAPO-11 material as a function of the synthesis parameters, keeping the following parameters constant: (a) $X_3 = 25$ mol, $X_4 = 0.02$ mol and $X_5 = 1.00$ mol; (b) $X_1 = 60$ h, $X_2 = 443$ K and $X_5 = 1.00$ mol; (c) $X_2 = 443$ K, $X_1 = 60$ h and $X_4 = 0.02$ mol.

3.3. Nature and location of vanadium in VAPO-11 and VAPO-41

We expect that the results of the experimental design are closely related to the molecular aspects of the vanadium incorporation in molecular sieves that in turn depends on the solution and solid state chemistry of vanadium. Information about the nature, co-ordination and location of the vanadium species present in our molecular sieves was obtained from the ESR spectra of the VAPO samples in the as-synthesized form. Some representative spectra are shown in Fig. 7. They are characteristic for well-dispersed and immobile V^{4+} species. Tetravalent vanadium is a system with $S = 1/2$ that displays a quite complex ESR spectrum, since there is a high number of hyperfine lines arising from the interaction of the unpaired d electron with the spin $I = 7/2$ of the 99.76% abundant ^{51}V nucleus. Due to the anisotropy of both g and A tensors, different spectral lines

overlap. Identical spectra were obtained at 298 and 150 K, indicating that the V^{4+} ions are not in T_d symmetry positions, since in the latter case, the ESR signals appear only at temperatures lower than 77 K and have low coupling constants [42]. Upon calcination of the samples in air at 773 K, the samples exhibit ESR spectra with very low intensity either at 298 or 150 K, due to the oxidation of V^{4+} to the ESR-silent V^{5+} species.

Most of the ESR signals have a rather horizontal baseline, indicating that there is no superimposed broad signal and therefore, most probably, no polynuclear oxidic vanadium is present. A rhombic symmetry has been proposed for the vanadium species present in the reported aluminophosphate sieves [24,43]. The g values and hyperfine coupling constants A have been obtained by simulating the spectra. The experimental and simulated ESR spectra coincide rather well with each other (Fig. 7). The corresponding g and A values are given in Table 4. These values are in

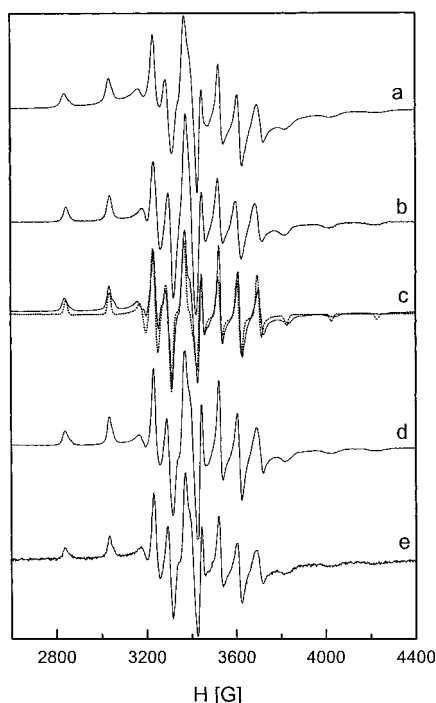


Fig. 7. ESR spectra of VAPO materials: (a) sample VAPO-41, (b) sample N16, (c) sample N24, (d) sample N6 and (e) sample VAPO-5. Dotted lines represent the simulated spectra.

good agreement with the values given in the literature for vanadium species as oxovanadium(IV) ions (vanadyl VO^{2+}) either in the aqueous complex

[47] or in related structures such as VAPO-5 [44–46] and VAPSO-44 [48]. In some cases, in order to obtain an adequate simulation, a broad Gaussian line with $g = 2.003$ and $\Delta H_{\text{pp}} = 300$ G had to be included.

The presence of vanadium as vanadyl species also results from the position of the obtained ESR parameters in the empirical correlation diagram of Davidson and Che [49]. The co-ordination around the V^{4+} ion is octahedral or square-pyramidal. Moreover, since the ESR parameters are quite similar, the local symmetry of vanadyl ions has to be rather similar in these samples, even though these have different structures. Indeed, both for the amorphous and crystalline VAPO materials, we obtain similar ESR parameters. This similarity of the local geometry might be another indication that vanadium is not entering into a true framework position, together with the fact that V^{4+} species with tetrahedral symmetry (namely, in a framework site) could not be observed by ESR technique as well as with the absence of protonated template resulting from the thermoanalytical measurements. At the same time, these vanadium species are strongly anchored to the aluminophosphate framework, since leaching experiments with solutions of ammonium acetate, known to eliminate vanadium polymeric surface species [50], have shown that the ESR signals are almost unaltered after such a treatment.

Table 4
ESR parameters of VAPO materials

Sample	g_{xx}	g_{yy}	g_{zz}	A_{xx} (G)	A_{yy} (G)	A_{zz} (G)	References
N6	1.983	1.974	1.935	74.8	66.4	197.4	This work
N21	1.983	1.975	1.936	74.5	63.4	197.1	This work
N23	1.981	1.973	1.931	76.5	66.4	199.6	This work
N24	1.980	1.977	1.932	72.2	70.4	199.7	This work
N26	1.983	1.975	1.933	77.4	68.4	200.1	This work
N16	1.982	1.973	1.937	69.8	67.2	197.6	This work
VAPO-41	1.985	1.971	1.935	73.4	69.6	196.2	This work
VAPO-5	1.984	1.972	1.935	71.2	69.0	199.4	This work
VAPO-5	1.996–1.991	1.996–1.991	1.936–1.931	73	73	198–201	[8]
VAPO-5	1.99	1.99	1.937	80	80	195	[7]
VAPO-5	1.983	1.983	1.932	78	78	198	[44]
VAPO-5	1.975	1.975	1.934	66	66	177	[47]
	1.975	1.975	1.927	66	66	175	
VAPO-5	1.993	1.977	1.947	74.2	74.2	196	[24]
VAPO-5	1.974	1.974	1.935	70.3	70.3	196	[46]

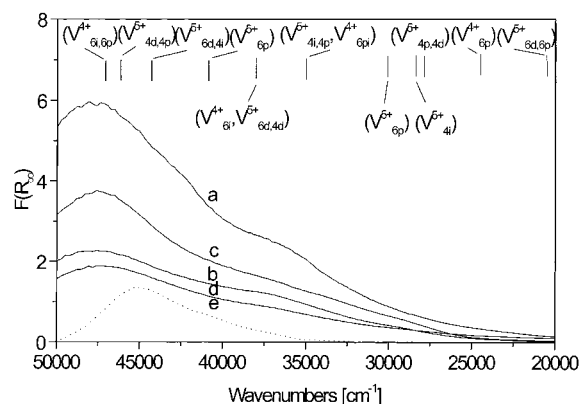


Fig. 8. DRS spectra of as-synthesized VAPO molecular sieves: (a) sample N3, (b) sample N5, (c) sample N17, (d) sample N23, (e) an AlPO-11 sample. The spectra were normalized for the vanadium content. Positions of absorption bands of reference compounds are also indicated, the symbols refer to vanadium valence (4+ or 5+), co-ordination (4 or 6) and polyhedron (i – isolated, d – dimer, p – polymer).

The occurrence of polynuclear oxidic vanadium species in the samples that show a lower amount of ESR-visible V^{4+} than vanadium amount found by elemental analysis (e.g. samples N17, N24) might be proven by DRS spectroscopy in the UV–VIS region. In Fig. 8, the DRS spectra for these samples are given along with those for the samples showing the same amount of vanadium by both elemental analysis and ESR methods (samples N3, N5). In the spectral region shown in this figure, there are charge transfer (CT) bands associated with an $O \rightarrow V$ electron transfer; the assignments of these bands, according to the literature [24,25], appear also in Fig. 8. One can see that the energies of the CT transitions are largely independent on the valence state of vanadium and that CT bands of the oligomeric (polymeric) species exhibit a red shift against those of the isolated species. However, the broad nature of the CT features makes it difficult to find the correct peak position and, consequently, to quantify the amount of polymeric species. In this respect, the absorption edge energies provide a more convenient description of the electronic properties of solids [51]. The position of the absorption edge is given in Fig. 9 as a function of the vanadium content. The edge energy decreases with increasing size of the vanadium clus-

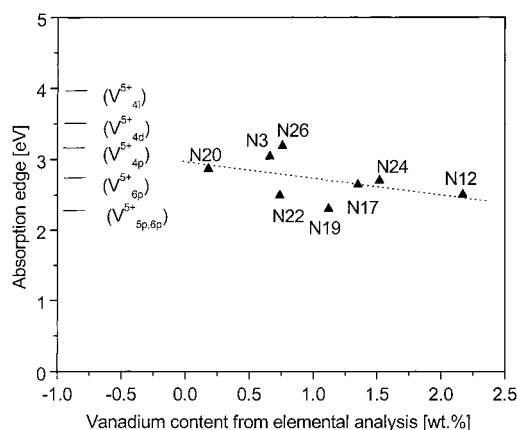


Fig. 9. Dependence of the UV–VIS absorption edge of VAPO materials on the vanadium content. Edge energies of reference compounds are also indicated, the symbols refer to vanadium co-ordination (4, 5 or 6) and polyhedron (i – isolated, d – dimer, p – polymer). The dotted line represents the least-squares fit at the data: $y = 2.96772 - 0.23668x$ ($R = -0.48609$, $SD = 0.28322$, $p = 0.22198$).

ters [31,52] till the value of 2.05 eV in the case of bulk V_2O_5 . At the same time, the higher the vanadium content, the higher the vanadium clustering. Samples N17 and N24 have a smaller edge energy than sample N3, therefore, they have to contain more polymeric forms than sample N3.

It results from the above that it is not obvious to conclude that vanadium ions are entering by isomorphous substitution the framework of the aluminophosphate molecular sieves under investigation (AEL and AFO). This has also been the conclusion for other aluminophosphate structures, such as AFI [24] and CHA [48]. In addition, this explains why some of the co-ordination models of the vanadium species proposed for vanadium containing microporous AlPO- n as well as for aluminosilicate molecular sieves are depicting vanadium as being anchored to the framework surface. Thus, Rigutto and van Bekkum [53] proposed that in vanadium containing silicalite, vanadium (as vanadyl VO^{2+}) is bonded to two framework oxygens, the other ligands around vanadium being OH groups bonded to silicon neighbors. In the models of Montes et al. [44] and Prakash and Kevan [54], vanadyl is anchored to the aluminophosphate framework by two bonds

with Al-O^- species. Because only two such framework aluminum atoms are neutralized, the other two framework aluminum atoms of the same T site remain to be neutralized by other cations and, therefore, the site where vanadium is bonded is a defect one. Three water molecules as ligands seem to co-ordinate to vanadyl to give a nearly octahedral symmetry observed for vanadium species, as deduced from ^2D ESEM spectra of the corresponding VAPO-5 samples [54]. The site is described with four V–O bonds in the equatorial plane and the vanadyl oxygen axially bonded along the z axis; the sixth ligand lies opposite the vanadyl oxygen. Another vanadium species proposed by Prakash and Kevan co-ordinates two framework oxygen atoms, two water molecules and a hydroxyl group [54], but in this case a protonated template has to compensate the additional negative charge. Due to the fact that related ligands, such as water, OH groups or framework O^{2-} cannot be distinguished by ESR, other models have four water molecules in the equatorial plane and a framework oxygen as the second axial ligand [25], but the anchoring is less strong than in the former case.

Vanadium complexes as described above to be anchored at the framework surface are already known from the solution chemistry of vanadium [55] and, therefore, they exist even in the initial synthesis gel. Moreover, the ESR spectra of two such vanadium species, namely of $\text{VO}(\text{H}_2\text{O})_5^{2+}$ and of $\text{VO}(\text{OH})(\text{H}_2\text{O})_4^+$, are quite similar, either at room temperature or in frozen solutions [56]. At high pH values, other species like $\text{VO}(\text{OH})_3(\text{H}_2\text{O})_2^-$ are formed [57], differing by coordination number (4–6) and hydration degree.

On the basis of the above data, it results that vanadium is rather strongly anchored to the surface of aluminophosphate molecular sieves, by bonds with the framework oxygens atoms. There are no tetrahedral vanadium(IV) species, but vanadyl ions as immobile and isolated species in pseudo-octahedral environment. This symmetry can be reached in defect sites of the framework. The model proposed by Prakash and Kevan [50], in which the $\text{V} = \text{O}^{2+}$ cation is attached to the surface with two framework oxygens and having three water molecules co-ordinated to the central

ion is the most plausible, even though we have not yet found evidence for the presence of protonated template molecules in the VAPO-11 and VAPO-41 materials, necessary to compensate for the charge balancing of the defect due to the vanadium linkages as well as for a possible OH^- ligand instead of one of the water ligands.

4. Conclusions

The hydrothermal synthesis of VAPO-11 molecular sieves and their physical mixtures with VAPO-41 has been achieved by using an experimental design with di- n -propylamine as the template molecule. Vanadium containing molecular sieves with the AEL structure can be obtained as a single phase; it may also be accompanied by the formation of AFO.

Experimental design was proved to be suitable in order to get the optimal synthesis conditions for obtaining single-phase AEL. The most important parameters allowing a control of the final product of the hydrothermal synthesis are a low vanadium content (i.e. 0.02 mol), a high water content (i.e. 25 mol) as well as a low synthesis temperature of 170°C and a long synthesis time of 60 h for autoclaving the synthesis gel.

Obtaining the molecular sieve with the AFO structure as a single phase was proved to be very difficult in the case of vanadium containing aluminophosphates, due to the additional requirements of synthesis, characteristic of the AFO structure, like seeding and controlling of the gel pH value.

The vanadium containing aluminophosphate molecular sieves were characterized by various physicochemical methods, including XRD, TGA, FTIR, SEM, ESR and DRS. ESR measurements have shown that vanadium species are immobile, mostly isolated and in a pseudooctahedral coordination. The spectra are characteristic for vanadyl compounds. These vanadium species exhibit similar ESR spectra no matter whether the corresponding sample is an amorphous material or a crystalline molecular sieve with different topologies. The ESR parameters were evaluated by performing accurate simulations of the spectra. These

parameters are in a good agreement with those found for vanadium incorporated in related materials. The amount of vanadium that can be incorporated in AlPO_4 -11 materials in isolated positions is limited to 1 wt.%. When the vanadium species are no more isolated, e.g., in the case of a higher vanadium loading, polymeric species were observed via the absorption edge in the DRS UV–VIS spectra.

Incorporation of vanadium into aluminophosphate molecular sieves takes place by co-ordination to two framework oxygens creating a defect site. A model of a surface complex containing six ligands around the vanadium central ion in a pseudo-octahedral co-ordination satisfactorily describes the data. The co-ordination of vanadium consists of the vanadyl oxygen, three oxygen atoms from water molecules and two oxygen atoms of the framework.

Acknowledgements

The authors acknowledge financial support from the Flemish Community under the bilateral agreement BIL 22/96 with Romania as well as from the Fonds voor Wetenschappelijk Onderzoek-Vlaanderen (FWO) and the Geconcerteerde Onderzoeksacties (GOA). B.M.W. and P.V.D.V. acknowledge the FWO for postdoctoral fellowships. The authors thank Hugo Leeman for technical assistance and Fina Pelgrims for preparing the scanning electron micrographs.

References

- [1] S.T. Wilson, B.M. Lok, C.A. Messina, T.R. Cannan, E.M. Flanigen, *J. Amer. Chem. Soc.* 104 (1982) 1146.
- [2] S.T. Wilson, E.M. Flanigen, *ACS Symp. Ser.* 398 (1989) 329.
- [3] S.T. Wilson, B.M. Lok, E.M. Flanigen, US Patent 4310440 (1982).
- [4] S.T. Wilson, B.M. Lok, E.M. Flanigen, US Patent 4 567 029 (1986).
- [5] M. Hartmann, L. Kevan, *Chem. Rev.* 99 (1999) 635.
- [6] B.M. Weckhuysen, R.R. Rao, J.A. Martens, R.A. Schoonheydt, *Eur. J. Inorg. Chem.* (1999) 565.
- [7] G. Blasco, P. Concepcion, J.M. Lopez Nieto, J. Perez-Pariente, *J. Catal.* 152 (1995) 1.
- [8] M.S. Rigutto, H. Van Bekkum, *J. Mol. Catal.* 81 (1993) 77.
- [9] S.H. Jung, Y.S. Uh, H. Chon, *Appl. Catal.* 62 (1990) 61.
- [10] P.S. Singh, K. Kosuge, V. Ramaswamy, B.S. Rao, *Appl. Catal. A* 177 (1999) 149.
- [11] D.E. Akporiaye, I.M. Dahl, A. Karlsson, R. Wendelbo, *Angew. Chem. Int. Ed.* 37 (1998) 609.
- [12] A. Holzwarth, H.W. Schmidt, W.F. Maier, *Angew. Chem. Int. Ed.* 37 (1998) 2644.
- [13] T. Bein, *Angew. Chem. Int. Ed.* 38 (1999) 323.
- [14] K. Choi, D. Gardner, N. Hilbrandt, T. Bein, *Angew. Chem. Int. Ed.* 38 (1999) 2891.
- [15] Q. Gao, B.M. Weckhuysen, R.A. Schoonheydt, *Micropor. Mesopor. Mater.* 27 (1999) 75.
- [16] A. Cichocki, P. Koscielniak, M. Michalik, M. Bus, *Zeolites* 18 (1997) 25.
- [17] A. Cichocki, P. Koscielniak, *Micropor. Mesopor. Mater.* 29 (1999) 369.
- [18] E. Dumitriu, D. Lutic, V. Hulea, D. Dorohoi, A. Azzouz, E. Colnay, C. Kappenstein, *Micropor. Mesopor. Mater.* 31 (1999) 187.
- [19] G. Øye, J. Sjöblom, M. Stöcker, *Micropor. Mesopor. Mater.* 34 (2000) 291.
- [20] R.M. Kirchner, J.M. Bennett, *Zeolites* 14 (1994) 523.
- [21] J.M. Bennett, J.W. Richardson, J.J. Pluth, J.V. Smith, *Zeolites* 7 (1987) 160.
- [22] H.J. Henson, A.K. Cheetham, *Chem. Mater.* 8 (1996) 664.
- [23] A. Navrotsky, *Mater. Res. Bull.* 22 (1997) 35.
- [24] B.M. Weckhuysen, I.P. Vanijvel, R.A. Schoonheydt, *Zeolites* 15 (1995) 482.
- [25] G. Catana, R.R. Rao, B.M. Weckhuysen, P. Van Der Voort, E.F. Vansant, R.A. Schoonheydt, *J. Phys. Chem. B* 102 (1998) 8005.
- [26] N.J. Tapp, N.B. Milestone, D.M. Bibby, *Zeolites* 8 (1988) 183.
- [27] A.M. Prakash, M. Hartmann, L. Kevan, *J. Phys. Chem. B* 101 (1997) 6819.
- [28] P. Meriaudeau, V.A. Tuan, V.T. Nghiem, S.Y. Lai, L.N. Hung, C. Naccache, *J. Catal.* 169 (1997) 55.
- [29] K. Dyrek, A. Rokosz, A. Madej, E. Bidzinska, *Appl. Magn. Reson.* 10 (1996) 319.
- [30] K.J. Mattson, R.B. Clarkson, R.L. Belford, 11th International EPR Symposium, 30th Rocky Mountain Conference, Denver, Colorado, 1988.
- [31] X. Gao, S.R. Bare, B.M. Weckhuysen, I.E. Wachs, *J. Phys. Chem. B* 102 (1998) 10842.
- [32] A.F. Ojo, L.B. McCusker, *Zeolites* 11 (1991) 460.
- [33] P.S. Singh, R. Bandyopadhyay, B.S. Rao, *J. Mol. Catal. A: Chemical* 104 (1995) 103.
- [34] M.C. Paganini, L. Dall'Acqua, E. Giamelo, L. Lietti, P. Forzatti, G. Busca, *J. Catal.* 166 (1997) 195.
- [35] M. Kovalakova, P.J. Grobet, *Appl. Magn. Reson.* 10 (1996) 447.
- [36] J. Kornatowski, G. Finger, K. Jancke, J. Richter-Mendau, D. Schultze, W. Joswig, W.H. Baur, *J. Chem. Soc. Faraday* 90 (1994) 2141.

- [37] J.B. Nagy, Z. Gabelica, E.G. Derouane, *Zeolites* 3 (1983) 43.
- [38] L.M. Parker, D.M. Bibby, J.E. Patterson, *Zeolites* 4 (1984) 168.
- [39] U. Lohse, R. Bertram, K. Janke, I. Kurzawski, B. Parltitz, E. Loeffler, E. Schreier, *J. Chem. Soc. Faraday Trans.* 91 (1995) 1163.
- [40] H.W. Clark, W.J. Rievert, M.M. Olken, *Micropor. Mater.* 6 (1996) 115.
- [41] A.M. Prakash, T. Wasowicz, L. Kevan, *J. Phys. Chem.* 100 (1996) 15947.
- [42] S. Di Gregorio, M. Greenblatt, J.H. Pifer, M.D. Sturge, *J. Chem. Phys.* 76 (1982) 2931.
- [43] M. Che, B. Canosa, A.R. Gonzalez-Elipse, *J. Phys. Chem.* 90 (1986) 618.
- [44] C. Montes, M.E. Davies, B. Murray, M. Narayana, *J. Phys. Chem.* 94 (1990) 6431.
- [45] D. Akolekar, R.F. Howe, in: H. Chou, S.K. Ihm, Y.S. Uh (Eds.), *Progress in Zeolite and Micropor. Mater.*, *Stud. Surf. Sci. Catal.*, vol. 105, Elsevier, Amsterdam, 1997, p. 755.
- [46] B.I. Whittington, J.R. Anderson, *J. Phys. Chem.* 97 (1993) 1032.
- [47] C.J. Ballhausen, H.B. Gray, *Inorg. Chem.* 1 (1962) 111.
- [48] U. Lohse, A. Brueckner, K. Kintser, B. Parltitz, E. Schreier, *J. Chem. Soc. Faraday Trans.* 91 (1995) 1173.
- [49] A. Davidson, M. Che, *J. Phys. Chem.* 96 (1992) 9909.
- [50] G. Centi, S. Perathorer, F. Trifiro, A. Abukais, C.F. Aissisi, M. Guelton, *J. Phys. Chem.* 96 (1992) 2617.
- [51] D. Wei, H. Wang, X. Feng, W.T. Chueh, P. Ravikovitch, M. Lyubovsky, C. Li, T. Takeguki, G.L. Haller, *J. Phys. Chem.* 103 (1999) 2113.
- [52] A. Khodakov, B. Olthof, A.T. Bell, E. Iglesia, *J. Catal.* 181 (1999) 205.
- [53] M.S. Rigutto, H. van Bekkum, *Appl. Catal.* 68 (1991) L1.
- [54] A.M. Prakash, L. Kevan, *J. Phys. Chem. B* 103 (1999) 2214.
- [55] N.N. Greenwood, A. Earnshaw, *Chemistry of the Elements*, Pergamon Press, Oxford, 1984.
- [56] J. Francavilla, N.D. Chasteen, *Inorg. Chem.* 14 (1975) 2860.
- [57] M.M. Ianuzzi, P.H. Rieger, *Inorg. Chem.* 14 (1975) 2895.